

Shape Memory Effect in Cu Nanowires

Wuwei Liang and Min Zhou*

School of Materials Science and Engineering, The George W. Woodruff School of Mechanical Engineering, Georgia Institute of Technology, Atlanta, Georgia 30332-0405

Fujju Ke

Department of Physics, Beijing University of Aeronautics and Astronautics, Beijing 100083, China

Received August 11, 2005

ABSTRACT

A rubber-like pseudoelastic behavior is discovered in single-crystalline face-centered-cubic (FCC) Cu nanowires in atomistic simulations. Nonexistent in bulk Cu, this phenomenon is associated primarily with a reversible crystallographic lattice reorientation driven by the high surface-stress-induced internal stresses due to high surface-to-volume ratios at the nanoscale level. The temperature-dependence of this behavior leads to a shape memory effect (SME). Under tensile loading and unloading, the nanowires exhibit recoverable strains up to over 50%, well beyond the typical recoverable strains of 5–8% for most bulk shape memory alloys (SMAs). This behavior is well-defined for wires between 1.76 and 3.39 nm in size over the temperature range of 100–900 K.

The pseudoelastic deformation of some shape memory alloys (SMAs) such as Au–Cd, Au–Cu–Zn, Cu–Zn–Al, and Cu–Al–Ni^{1–3} proceeds through the reversible movement of twin boundaries. The behavior of these materials is commonly referred to as rubber-like because of its resemblance to the behavior of soft and pseudoelastic rubber.⁴ A similar behavior and a SME are discovered in single-crystalline Cu nanowires through atomistic simulations. This behavior at the nanoscale level is due to reversible crystallographic lattice reorientations through the movement of twin boundaries, allowing Cu nanowires to exhibit recoverable strains of up to 50%, which are well beyond the recoverable strains of 5–8% of most SMAs. This phenomenon occurs only in nanowires within the size range of 1.76–3.39 nm and is not observed in bulk Cu. Furthermore, it is temperature-dependent and hence gives rise to an SME. Specifically, the critical temperature for spontaneous reorientation upon unloading increases from 100 to 900 K as the wire size increases from 1.76 to 3.39 nm, making it possible to design nanoscale components of varying sizes for operation over a wide range of temperature. Such an objective is more difficult to achieve with conventional bulk SMAs because their transition temperatures (martensite start and finish temperatures, austenite start and finish temperatures) vary only with material structure and composition, not size. Moreover, the nanowires analyzed here have very short response times that are on the order of nanoseconds because of their extremely

small dimensions compared to bulk SMAs. These unique properties can lead to important applications at the nanoscale level including sensors, transducers, and actuators in nanoelectromechanical systems (NEMS).^{5,6}

The analysis here focuses on Cu nanowires created experimentally through a “top-down” fabrication approach.⁷ These wires have a single-crystalline FCC structure with a $\langle 110 \rangle$ axis and $\{111\}$ transverse surfaces (hereafter denoted as the $\langle 110 \rangle / \{111\}$ wire or configuration). This configuration represents a low energy state for FCC metallic nanowires and has been observed frequently in experiments and atomistic simulations for Au, Cu, and Ag nanowires.^{7–12} The specific nanowires analyzed are created computationally in the spirit of the top-down fabrication process by “slicing” square columns of atoms from single-crystalline bulk Cu along the [001], [010], and [100] directions and by allowing them to undergo relaxation. Driven by surface stresses, the nanocolumns spontaneously transform into the $\langle 110 \rangle / \{111\}$ configuration through a lattice reorientation process, exhibiting a contraction in the axial direction and an expansion in the lateral directions. The resulting free-standing wires have the same FCC structure as that of bulk Cu at the same temperature,¹³ with a rhombic cross-sectional shape as shown in Figure 1a. In this paper, the side length, l_0 , of the rhombic cross-sections (Figure 1a) is used to identify the wire size. All of the simulations reported here are performed using the embedded-atom method (EAM) potential for Cu,¹⁴ although similar results are obtained using other potentials as discussed later.

* Corresponding author. Tel: 404-894-3294. Fax: 404-894-0186. E-mail: min.zhou@me.gatech.edu.

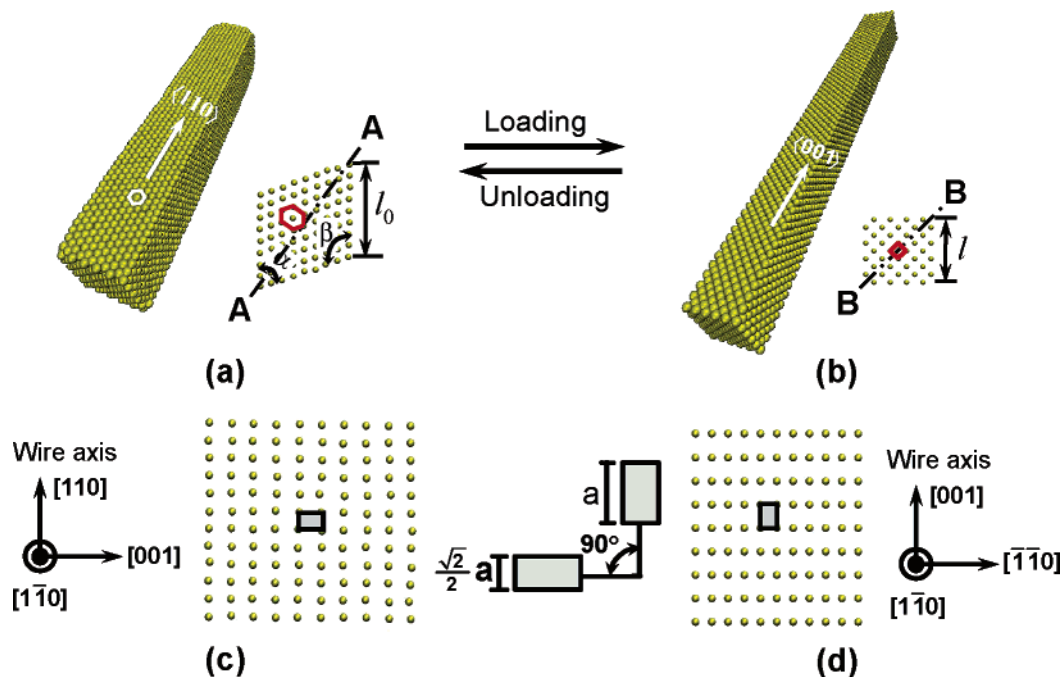


Figure 1. Reversible lattice reorientations upon loading and unloading in single-crystalline Cu nanowires; (a) original $\langle 110 \rangle / \{ 111 \}$ wire with rhombic cross-sections, $\alpha = 70.5^\circ$ and $\beta = 109.5^\circ$, (b) stretched $\langle 001 \rangle / \{ 001 \}$ wire with square cross-sections, (c) (110) atomic plane containing the $[110]$ wire axis and the long diagonal AA ($[001]$) of the rhombic cross-section in the original wire, (d) the same $(1\bar{1}0)$ atomic plane after lattice reorientation, containing the new wire axis ($[001]$) and the diagonal BB ($[1\bar{1}0]$) of the new square cross-section.

To analyze the wires' mechanical behavior, we carried out uniaxial tensile loading and unloading under simulated quasi-static conditions.¹⁵ Specifically, in each load step, all of the atoms are first displaced according to a prescribed uniform strain increment of 0.125% in the length direction. The wires are then relaxed with their ends fixed at constant temperature for 9 picoseconds (ps) to obtain a macroscopic equilibrium configuration at the prescribed strain. This relaxation process allows structural changes to occur, if the conditions so dictate. This process usually takes less than 6 ps, and the averaged stress over the last 3 ps of the relaxation period at each load step is taken as the stress in the wire at the current strain. Unloading is implemented in the same manner, with a negative strain increment of -0.125% .

Upon uniaxial loading and unloading, wires with lateral dimensions between 1.76×1.76 and 3.39×3.39 nm² exhibit a pseudoelastic behavior above a critical temperature, T_{cr} (discussed later), with large recoverable strains of up to 50% or more. Below T_{cr} , the deformation is not spontaneously recoverable and the wires retain their deformed configurations after unloading.

Figure 2 shows the stress–strain curve of a $\langle 110 \rangle / \{ 111 \}$ wire with a lateral dimension of 1.76×1.76 nm² during loading and unloading at 200 K. Clearly, the response is drastically different from that of bulk Cu. Specifically, the nanowire seems highly ductile with a fracture strain of approximately 58%. The stress–strain curve consists of two linear deformation stages (O \rightarrow A and C \rightarrow D) followed by two yield points (A and D, respectively), a stage of slow strain hardening over a wide range of strain (B \rightarrow C), and a stage of precipitous stress drop (D \rightarrow E). This behavior arises from a unique underlying deformation process. Between O

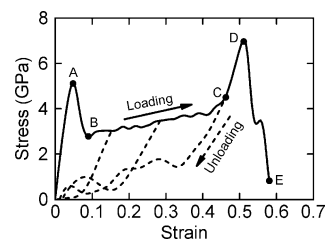


Figure 2. Stress–strain curve of a 1.76×1.76 nm² Cu nanowire during loading and unloading at 200 K.

and A, the $\langle 110 \rangle / \{ 111 \}$ wire undergoes elastic stretching. Point A corresponds to the beginning of a lattice reorientation process that leads to a new configuration with a $\langle 001 \rangle$ axis and $\{ 001 \}$ side surfaces (hereafter denoted as the $\langle 001 \rangle / \{ 001 \}$ wire or configuration), as shown in Figure 1b. Between C and D, the newly formed $\langle 001 \rangle / \{ 001 \}$ wire undergoes elastic stretching. Further loading beyond D causes the wire to yield through the formation and propagation of partial dislocations, which ultimately lead to necking and fracture of the nanowire at E.¹⁶

The unique lattice reorientation process (between point A and C in Figure 2) is completed through the propagation of a twin boundary. Specifically, the twin boundary is formed through the propagation of a $(1/6) \langle 112 \rangle$ Shockley partial dislocation nucleated from an edge at the lower end. This partial dislocation glides across the wire on a $\{ 111 \}$ plane and leaves behind the twin boundary. Under the tensile loading, the twin boundary sweeps through the wire length and progressively transforms the wire into a new $\langle 001 \rangle$ orientation, as shown in Figure 3. Clearly, the twin boundary divides the wire into two domains: one with the initial $\langle 110 \rangle / \{ 111 \}$ configuration and the other with the $\langle 001 \rangle / \{ 001 \}$

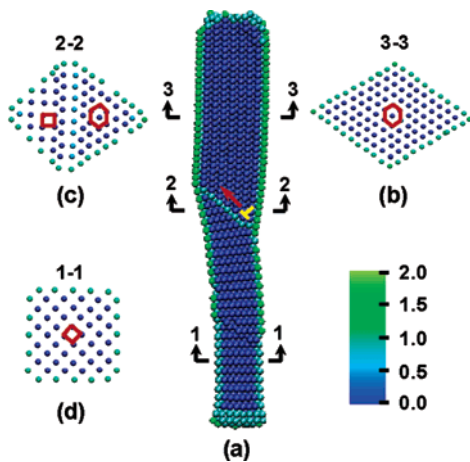


Figure 3. Lattice orientations on the cross sections of a $1.76 \times 1.76 \text{ nm}^2$ Cu nanowire at a strain of 0.24; (a) a sectional view along the wire axis and the $\langle 110 \rangle$ diagonal of the cross section, (b) elongated hexagonal lattice on the cross section in the unrotated domain with the $\langle 110 \rangle/\{111\}$ configuration, (c) a cross section in the transition region containing both the $\langle 001 \rangle/\{001\}$ and the $\langle 110 \rangle/\{111\}$ configurations, (d) square lattice on the cross section in the rotated domain with the $\langle 001 \rangle/\{001\}$ configuration. Atoms are colored according to their centrosymmetry values.

configuration, as shown in Figure 3. A cross section intersecting the twin boundary shows the lattice transition between the two domains clearly (Figure 3c). Upon the arrival of the boundary at the top end of the wire (corresponding to point C in Figure 2), the whole wire is in the $\langle 001 \rangle/\{001\}$ state without residual defects. The reversibility of the lattice reorientation from $\langle 110 \rangle/\{111\}$ to $\langle 001 \rangle/\{001\}$ allows the associated deformation to be recovered fully upon unloading, giving rise to a pseudoelastic behavior of the wire. Specifically, the $\langle 001 \rangle/\{001\}$ wire transforms back to the original $\langle 110 \rangle/\{111\}$ configuration via a lattice reorientation process in reverse to what is described above for loading. The dashed lines in Figure 2 represent the unloading paths from three different strains (0.05, 0.30, and 0.464, respectively). Clearly, the deformations are recovered fully when the stress is reduced to zero. The loading and unloading paths together form hysteresis loops typical of shape memory materials.⁴

The forward (loading) and reverse lattice reorientation (unloading) processes are critical to the SME of the wires because they result in a 41.4% recoverable strain (discussed later). Both processes have been confirmed by experiments. Specifically, FCC nanowires are found to undergo the same forward reorientation during tensile deformation in high-resolution transmission electron microscope (HRTEM) experiments.¹⁷ The spontaneous reverse reorientation process has also been observed in various experiments and computations.^{7,8,13,18–20} The same result is also obtained in computations when different atomistic potentials (including an EAM, a modified embedded atom method (MEAM), and a surface-embedded atom potential (SEAM)) are used.⁸

The large strain associated with the forward and reverse lattice reorientations between A and C in Figure 2 can be quantified by a simple crystallographic analysis. Figure 1(c and d) compares the same $(1\bar{1}0)$ plane in the original

undeformed $\langle 110 \rangle/\{111\}$ configuration and the deformed $\langle 001 \rangle/\{001\}$ configuration. Clearly, the forward and backward lattice reorientations manifest as 90° rotations in opposite directions of the unit cell in the $(1\bar{1}0)$ plane. The length and width of the rectangular unit cell in both cases are, respectively, a and $(\sqrt{2}/2)a$; where a is the lattice constant in the stressed states and is assumed to be the same at A and C. The axial strain associated with the lattice reorientation between A and C is given by

$$\epsilon_{\langle 110 \rangle \leftrightarrow \langle 001 \rangle} = \frac{a - \frac{\sqrt{2}}{2}a}{\frac{\sqrt{2}}{2}a} = 0.414 \quad (1)$$

This value of $\epsilon_{\langle 110 \rangle \leftrightarrow \langle 001 \rangle}$ is consistent with the value obtained in simulations, as shown in Figure 2. This strain, along with the elastic strain, $\epsilon_{\langle 110 \rangle}^e$, associated with the lattice stretching in the $\langle 110 \rangle/\{111\}$ configuration between O and A (Figure 2) and the elastic strain, $\epsilon_{\langle 001 \rangle}^e$, associated with the lattice stretching in the $\langle 001 \rangle/\{001\}$ configuration between C and D, constitutes the total pseudoelastic strain of

$$\epsilon_r \approx \epsilon_{\langle 110 \rangle}^e + \epsilon_{\langle 110 \rangle \leftrightarrow \langle 001 \rangle} + \epsilon_{\langle 001 \rangle}^e = 0.05 + 0.414 + 0.05 = 0.514 \quad (2)$$

This recoverable strain is essentially the same for all wires with lateral dimensions between 1.76×1.76 and $3.39 \times 3.39 \text{ nm}^2$ and endows the nanowires with the ability for pseudoelastic elongations of up to 51.4%, which is many times the typical 5–8% recoverable strains for most bulk SMAs.²²

Note that the pseudoelastic behavior of SMAs arise from two related but somewhat different mechanisms that yield very similar stress–strain relations such as that in Figure 2. The first mechanism is rubber-like and occurs solely within the martensitic state through reversible movement of twin boundaries.⁴ The second mechanism is superelastic and involves an austenite-to-martensite phase transformation. Clearly, the mechanism responsible for the pseudoelastic behavior of the nanowires analyzed here is more rubber-like than superelastic because the deformation occurs through twin boundary propagation solely within the FCC structure, without any phase change. Although the rubber-like behavior is often seen in bulk SMAs with appropriate aging in the martensitic state and necessary lattice imperfections,³ neither aging nor lattice imperfections are involved in the rubber-like behavior of the Cu nanowires. The behavior of the nanowires also bears striking resemblance to the rubber-like behavior of solid-state polymers (e.g., Jell-O) in terms of the stress–strain relation and morphological changes. Specifically, the stress–strain curves of both are characterized by an initial yield point followed by a stress plateau and a terminal stress increase that leads to eventual failure.²³ In addition, both deform via the reorientation of their micro- or nanostructure. However, compared to solid-state polymers, the nanowires have high strength and excellent thermal and electrical conductivities.

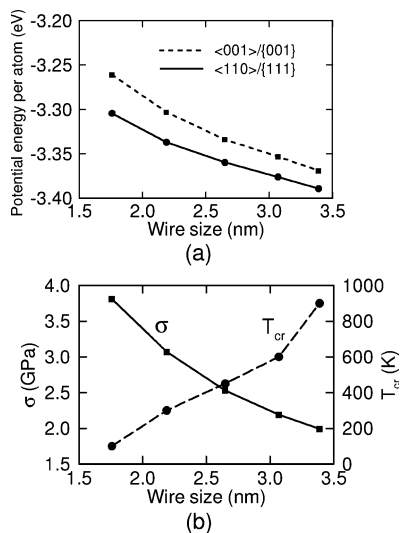


Figure 4. (a) Comparison of the potential energy per atom of wires with the $\langle 110 \rangle / \{ 111 \}$ and $\langle 001 \rangle / \{ 001 \}$ configurations at 300 K, (b) variations of surface-stress-induced compressive stress σ and the critical temperature, T_{cr} , with wire size.

What causes the $\langle 001 \rangle / \{ 001 \}$ wire to spontaneously revert back to its original $\langle 110 \rangle / \{ 111 \}$ configuration upon unloading, because both states have the same FCC crystalline structure and, perhaps, the same “stability”? The answer lies in the surfaces and the extremely high surface-to-volume ratios of nanowires that can affect structural stability significantly. Specifically, the surface energy is 1.280 Jm^{-2} for $\{ 001 \}$ planes and 1.17 Jm^{-2} for $\{ 111 \}$ planes,¹⁴ causing the $\langle 110 \rangle / \{ 111 \}$ configuration to have a lower energy and to be more stable compared to the $\langle 001 \rangle / \{ 001 \}$ configuration. A quantification of the difference in the potential energy as a function of wire size between the two configurations is given in Figure 4a. This energy difference results primarily from the energy density difference between $\{ 111 \}$ and $\{ 001 \}$ surfaces. The average potential energy per atom decreases with increasing wire size for each configuration because smaller wires have larger surface-to-volume ratios. However, regardless of size, $\langle 110 \rangle / \{ 111 \}$ wires always have lower energy levels compared to their deformed counterparts with the $\langle 001 \rangle / \{ 001 \}$ configuration. Therefore, the $\langle 001 \rangle / \{ 001 \}$ wire has a natural tendency for spontaneous reorientation back to the $\langle 110 \rangle / \{ 111 \}$ configuration upon unloading. The reorientation essentially lowers the surface energy as a result of the increase in atomic density on surfaces when $\{ 001 \}$ surfaces reorganize into closely packed $\{ 111 \}$ surfaces.

The driving force for the spontaneous reorientation can also be viewed as coming from the surface stress that induces a compressive stress in the interior of the wire. This compressive stress is $\sigma = -4f/lA$, where f is the surface stress of the $\{ 001 \}$ planes in the $\langle 001 \rangle / \{ 001 \}$ configuration, l is the side length of the square cross-section (Figure 1b), and $A (= l^2)$ is the corresponding cross-sectional area.^{15,19} Obviously, the magnitude of σ increases as the wire size decreases and can be very high at the nanoscale level, as shown in Figure 4b. For example, $\sigma = -3.81 \text{ GPa}$ for a $\langle 001 \rangle / \{ 001 \}$ wire with $l = 1.45 \text{ nm}$ ($l_0 = 1.76 \text{ nm}$ in the $\langle 110 \rangle / \{ 111 \}$ state), sufficient for initiating the reverse

reorientation at temperatures above 100 K, even in the absence of externally applied forces. Note, however, that σ is only on the order of Pascals in bulk materials and is negligible, providing an explanation as to why a similar behavior is not seen in bulk Cu.

Similar to the behavior of normal bulk SMAs, the pseudoelastic behavior reported here is strongly temperature-dependent. Specifically, the reverse lattice reorientation from $\langle 001 \rangle$ to $\langle 110 \rangle$ occurs only above a size-dependent critical temperature, T_{cr} (Figure 4). If unloading takes place at temperatures below T_{cr} , then the reverse lattice reorientation does not occur and the wire retains the $\langle 001 \rangle / \{ 001 \}$ configuration. When subsequently heated above T_{cr} , the unloaded $\langle 001 \rangle / \{ 001 \}$ wire spontaneously returns to its original $\langle 110 \rangle / \{ 111 \}$ configuration through the reverse lattice reorientation. This is a novel SME driven by surface stress and the high surface-to-volume ratios of the nanowire. It is a one-way SME that has the $\langle 110 \rangle / \{ 111 \}$ configuration as the parent state.

If the $\langle 110 \rangle / \{ 111 \}$ state always has a lower energy than the corresponding $\langle 001 \rangle / \{ 001 \}$ state regardless of size, then why does the reverse reorientation occur only above T_{cr} ? The answer has to do with the energetic barrier and driving force of the process. Partial dislocations nucleate and propagate to accommodate mobile twin boundaries to initiate the reorientation. These defects are of higher energies and thus constitute an energy barrier for the reorientation. Thermal energy can provide the necessary energy for overcoming the barrier.²⁴ As wire size increases, σ decreases and higher temperatures are needed to initiate the spontaneous reverse reorientation, as shown in Figure 4b. For example, T_{cr} is 100 K for a $1.76 \times 1.76 \text{ nm}^2$ wire and 900 K for a $3.39 \times 3.39 \text{ nm}^2$ wire. For wires thicker than $3.39 \times 3.39 \text{ nm}^2$, T_{cr} approaches a significant fraction of the melting point. Under such conditions, the pseudoelastic behavior and the SME are no longer obvious because the wire behavior becomes disorganized and dominated by random atomic vibrations. Because of this reason, the well-defined rubber-like pseudoelasticity and SME exist only in Cu nanowires with lateral dimensions below 3.39 nm .

In summary, the temperature dependence of the rubber-like pseudoelastic behavior in single-crystalline Cu nanowires leads to an SME that is well-defined for sizes between 1.76 and 3.39 nm over the temperature range of 100–900 K. Tensile strains up to 50% can be recovered. The responsible mechanism is a reversible lattice reorientation driven by the high surface-stress-induced internal stresses at the nanometer scale, explaining why such a behavior is not observed in Cu at higher scales. This unique behavior makes Cu nanowires attractive functional components for biosensors, transducers, actuators, and interconnects in NEMS.

Acknowledgment. This research is supported by NASA Langley Research Center through grant no. NAG-1-02054. Computations are carried out at the NAVO, ARL, and ERDC MSRCs through AFOSR MURI no. D49620-02-1-0382. The work of FJK is supported by grant no. 10372012 of the NSFC.

References

- (1) Christian, J. W. *Metall. Trans.* **1982**, *13A*, 509–538.
- (2) Cahn, R. W. *Nature* **1995**, *374*, 120–121.
- (3) Ren, X.; Otsuka, K. *Nature* **1997**, *389*, 579–582.
- (4) Otsuka, K.; Wayman, C. M. *Shape Memory Materials*; Cambridge University Press: New York, 1998; p 282.
- (5) Otsuka, K.; Kakeshita, T. *MRS Bull.* **2002**, *Feb*, 91–98.
- (6) Büttgenbach, S.; Büttefish, S.; Leester-Schädel, M.; Wogersien, A. *Microsyst. Technol.* **2001**, *7*, 165–170.
- (7) Kondo, Y.; Takayanagi, K. *Phys. Rev. Lett.* **1997**, *79*, 3455–3458.
- (8) Diao, J.; Gall, K.; Dunn, M. L. *Phys. Rev. B* **2004**, *70*, 075413.
- (9) Liu, Z.; Yang, Y.; Liang, J.; Hu, Z.; Li, S.; Peng, S.; Qian, Y. *J. Phys. Chem. B* **2003**, *107*, 12658–12661.
- (10) Liu, Z.; Bando, Y. *Adv. Mater.* **2003**, *15*, 303–305.
- (11) Diao, J.; Gall, K.; Dunn, M. L. *Nano Lett.* **2004**, *4*, 1863–1867.
- (12) Rodrigues, V.; Ugarte, D. Structural study of metal nanowires. In *Nanowires and Nanobelts: Materials, Properties and Devices*; Wang, Z. L., Ed.; Springer: New York, 2003; pp 177–209.
- (13) Liang, W.; Zhou, M. *J. Eng. Mater. Technol.* **2005**, *127*, 423–433.
- (14) Foiles, S. M.; Baskes, M. I.; Daw, M. S. *Phys. Rev. B* **1986**, *33*, 7983–7991.
- (15) Gall, K.; Diao, J.; Dunn, M. L. *Nano Lett.* **2004**, *4*, 2431–2436.
- (16) Liang, W.; Zhou, M. *J. Mech. Eng. Sci.* **2004**, *218*, 599–606.
- (17) Rego, L. G. C.; Rocha, A. R.; Rodrigues, V.; Ugarte, D. *Phys. Rev. B* **2003**, *67*, 045412.
- (18) Kondo, Y.; Ru, Q.; Takayanagi, K. *Phys. Rev. Lett.* **1999**, *82*, 751–754.
- (19) Diao, J.; Gall, K.; Dunn, M. *Nat. Mater.* **2003**, *2*, 656–660.
- (20) Hasmy, A.; Medina, E. *Phys. Rev. Lett.* **2002**, *88*, 096103.
- (21) Ohnishi, H.; Kondo, Y.; Takayanagi, K. *Nature* **1998**, *395*, 780–783.
- (22) Otsuka, K.; Ren, X. *Intermetallics* **1999**, *7*, 511–528.
- (23) Ward, I. M. *Mechanical Properties of Solid Polymers*, 2nd ed.; John Wiley & Sons: New York, 1983; pp 15–26.
- (24) Meyers, M. A. *Mechanical Metallurgy: Principles and Applications*; Printice-Hall Inc.: Englewood Cliffs, NJ, 1984; pp 320–327.

NL0515910